Architecture-dependent interplay between self-assembly and crystallization in discrete block co-oligomers

ACS Macro Letters

Letter

Cite This: ACS Macro Lett. 2020, 9, 38−42

pubs.acs.org/macroletters

Architecture-Dependent Interplay between Self-Assembly and Crystallization in Discrete Block Co-Oligomers

Katja Petkau-Milroy,*[,†] Alessandro Ianiro,[‡,§] Melanie M. L. Ahn,[†] Jose Rodrigo Magana,[‡,∥] Marle E. J. Vleugels,[†] Brigitte A. G. Lamers,[†] Remco Tuinier,[‡,§] Ilja K. Voets,[‡,∥] Anja R. A. Palmans,*[,†,‡] and E. W. Meijer*[,†,‡]

[†]Laboratory of Macromolecular and Organic Chemistry, [‡]Institute for Complex Molecular Systems, [§]Laboratory of Physical Chemistry, and [∥]Laboratory of Self-Organizing Soft Matter. Eindhoven University of Technology, P.O. Box 513, 5600 MB Eindhoven, The Netherlands

Supporting Information

ABSTRACT: Access to versatile and stable nanostructures formed by the self-assembly of block copolymers in water is essential for biomedical applications. These applications require control over the stability, morphology, and size of the formed nanostructures. Here, we study the self-assembly in water of a library of fully discrete and sequence-controlled AB-type block co-oligomers (BCOs) of oligo(L-lactic acid)-*b*-oligo(ethylene glycol). In this series, we eliminate all the inherent uncertainty associated with molar mass, ratio, and compositional dispersity, but vary the ratio between the water-soluble and water-insoluble parts. The BCO library is designed in such a way that vesicles, spherical micelles, and cylindrical micelles are generated in solution, hereby covering a variety of common morphologies. With the help of self-consistent field (SCF) computations, the thermodynamic structures in water are predicted for all structures. The morphologies formed were experimentally analyzed using a combination of calorimetry and scattering techniques. When comparing the experimentally found structures with those predicted, we find an excellent agreement. Intriguingly, calorimetry showed the presence of crystallized L-lactic acid (LLA) units in the bilayer of the lamellar forming BCO. Despite this crystallinity, there is no mismatch between the predicted and observed bilayer thicknesses upon self-assembly in water. In this case, phase separation driven by the hydrophobic LLA block coincides with crystallization, resulting in stable morphologies. Thus, SCF guided library design and sample preparation can lead toward robust formulations of nanoparticles.

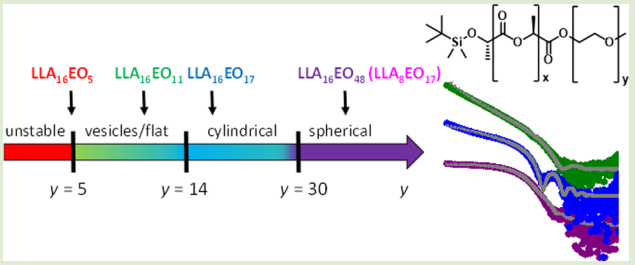

The versatility and tuneability of block copolymer (BCP) assembly into a wide variety of supramolecular morphologies make BCPs interesting building blocks for a plethora of applications, ranging from nanolithography to drug delivery.[1−4] By varying the chemical composition of the monomers and the length of BCP blocks, new materials with emerging properties and adjustable structures can be designed.[5] Amphiphilic BCPs can form bulk structures with long-range periodicity as well as colloidal nanostructures in selective solvents (e.g., vesicles, spherical micelles, and cylindrical micelles).[6] Immiscibility of the blocks drives the microphase separation in bulk, while (un)favorable interactions with solvent molecules play a key role in the self-assembly process in solution. The latter results in core−corona structures, wherein the core is composed of collapsed lyophobic chains.[7] Often, BCP assembly is (partially) kinetically trapped, so that the final supramolecular structure depends both on thermodynamic factors (such as block length and composition) and kinetic factors (such as the preparation pathway).[8,9] The thermodynamic equilibrium structure may be accessible via one route, but prohibitively blocked via another to yield a kinetically trapped metastable state instead. For biomedical applications, such as drug delivery, a high degree of understanding and control over the morphology, size, and stability of nanostructures are crucial.[10−12] Several predictive methods, for example, self-consistent field (SCF) computations, have shown their potential to predict equilibrium morphologies and sizes as a function of BCP composition. As a result, they can be used not only to guide the synthetic design, but also the sample preparation toward thermodynamic equilibrium structures.[13]

For low molecular weight block-*co*-oligomers (BCOs), it was observed that dispersity has a dramatic effect on the homogeneity of microphase separation in bulk,[14−19] as well as on the homogeneity of self-assembly in water.[20,21] Here, we study the behavior of fully discrete and sequence-controlled AB-type BCOs in bulk and in water, thus, eliminating all the inherent uncertainty associated with molar mass, ratio, and compositional dispersity. The microphase separation and crystallization behavior of BCOs are studied by means of

Received: October 18, 2019
Accepted: December 6, 2019
Published: December 12, 2019

DOI: 10.1021/acsmacrolett.9b00814
ACS Macro Lett. 2020, 9, 38−42

scattering and calorimetry. The prediction of the solution self-assembly using the Scheutjens-Fleer SCF theory[22] computations is used to guide the sample preparation with the aim to arrive at the thermodynamic equilibrium. The final self-assembled structures ranging from spherical to cylindrical micelles, and vesicles are analyzed with multiangle laser light scattering, small and wide-angle X-ray scattering (SAXS and WAXS), total internal reflection fluorescence (TIRF) microscopy, and differential scanning calorimetry (DSC), and compared to the SCF predictions.

Discrete oligomers of L-lactic acid (LLA), TBDMS-LLA_8-COOH and TBDMS-LLA_{16}-COOH, were obtained via a slight modification of the procedures previously reported by Hawker's group (Scheme S1).[23] Subsequent ligation with commercially available discrete ethylene oxide (EO) oligomers MeO-EO_y-OH (n = 5, 11, 17, and 48) resulted in a set of five discrete BCOs (Figure 1a). All compounds were purified by

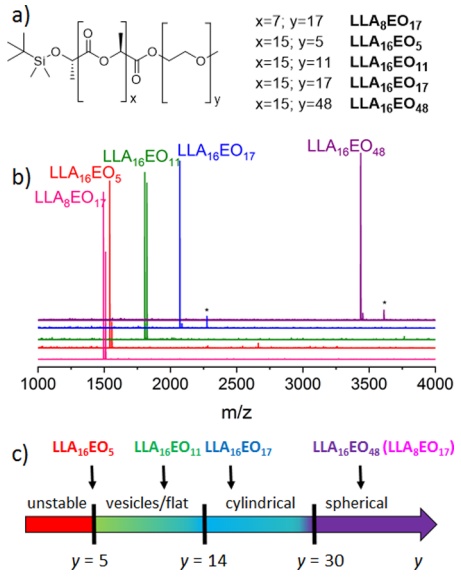

Figure 1. (a) Chemical structures of the discrete BCOs; (b) MALDI-ToF spectra of the BCO library; * is a CHCA matrix artifact; (c) SCF predicted self-assembled morphologies for $LLA_{16}EO_n$ in water.

automated column chromatography and fully analyzed by ^{1}H NMR, ^{13}C NMR, and matrix-assisted laser desorption/ionization time-of-flight (MALDI-ToF) mass spectrometry (Figures S1–S7). The TBDMS group was not removed, mainly to increase the stability of the BCOs. A terminal hydroxyl group of PLA leads to fast stepwise chain end scission through intramolecular attack of the penultimate ester bond.[24,25] TBDMS-protected oligomers of lactic acid degrade slower through a random chain scission mechanism (Figures S8 and S9). Additionally, the hydrophobic nature of TBDMS should aid the self-assembly process in water. The single peaks in the MALDI-ToF spectra underline the discreteness of the studied BCOs and are indicative of their high purity (Figure 1b). This discrete nature makes it possible to easily follow the stability/degradation of self-assembled BCOs over time (Figures S10 and S11). The details of the preparation of BCOs and the stability/degradation studies can be found in the Supporting Information.

The thermal behavior and degree of ordering in the bulk of $LLA_{16}EO_y$ were investigated using DSC and WAXS (Table 1, Table S1, Figures 2 and S12). Discrete oligomers of L-lactic

Table 1. Appearance, Thermal Properties, and Observed Bulk Morphologies of the BCOs

BCO	appearance[a]	T_m (°C)	T_c (°C)	ΔH_{Tc} (kJ/mol)	phase[b]	d^*[c] (nm)
$LLA_{16}EO_5$	wax	69	none	none	LAM	6.5
$LLA_{16}EO_{11}$	wax	50	22	32	LAM	7.9
$LLA_{16}EO_{17}$	wax	51	32	43	LAM	9.2
$LLA_{16}EO_{48}$	solid	48	−10, 27	152, 28	n.d.	22.4

[a]Physical appearance at room temperature, directly after drying in vacuo. [b]Bulk morphology determined with WAXS at room temperature. LAM = lamellar, n.d. = not determined. [c]Domain spacing, calculated as $d^* = 2\pi/q^*$.

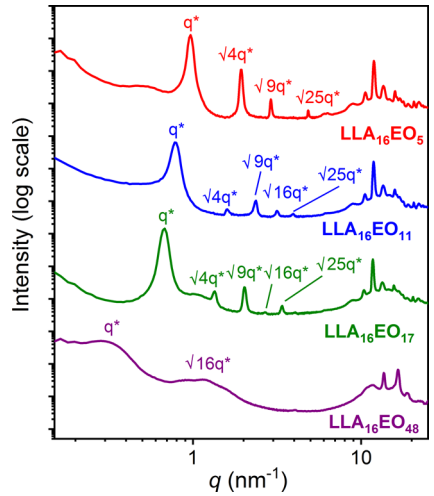

Figure 2. Wide-angle X-ray scattering data for $LLA_{16}EO_5$ (red), $LLA_{16}EO_{11}$ (blue), $LLA_{16}EO_{17}$ (green), and $LLA_{16}EO_{48}$ (purple). Data is shifted vertically for clarity. Higher order Bragg reflections are indicated if present.

acid were shown to crystallize in bulk if the chain length is ≥16, and indeed, LLA_8EO_{17} did not crystallize.[17] In addition, the length of the oligo(ethylene oxide) chains (EO_y) also affects the thermal behavior of these crystalline oligomers. Longer EO_y chains are known to crystallize in bulk,[26,27] and for $LLA_{16}EO_{48}$, two crystallization transitions are observed upon cooling. These transitions can be ascribed to the crystallization of LLA_{16} and of EO_{48}. Upon heating, the longer EO_n chains do not affect the behavior of the BCOs since the melting transitions do not change (50 vs 48 °C for $LLA_{16}EO_{17}$ vs $LLA_{16}EO_{48}$, respectively; Table 1 and Figure S12a). X-ray scattering profiles (Table 1, Figure 2) for $LLA_{16}EO_5$, $LLA_{16}EO_{11}$, and $LLA_{16}EO_{17}$ display sharp principal scattering peaks and higher order Bragg reflections, indicating a highly ordered phase-separated structure. The ratios of the Bragg reflections ($\sqrt{4}$, $\sqrt{9}$, $\sqrt{16}$, $\sqrt{25}$) indicate a lamellar phase (LAM). Furthermore, multiple scattering peaks can be observed in the WAXS region, corresponding to d-spacings characteristic for crystalline packing of the lactic acid chain.[28] In contrast, the $LLA_{16}EO_{48}$ bulk phase appears more disordered as less and broader Bragg reflections are observed. This indicates that EO_{48} crystallization interferes with phase separation. The ability of the longest EO_{48} chain to crystallize is also seen in the WAXS data of $LLA_{16}EO_{48}$. At higher q-

DOI: 10.1021/acsmacrolett.9b00814
ACS Macro Lett. 2020, 9, 38–42

Table 2. Comparison between Predicted and Scattering Results of the Self-Assembled BCOs in Water

	prediction based on SCF			actual measurements		
BCO	shape	R_{core} [a] (nm)	R [b] (nm)	shape	R_H [c] (nm)	R [d] (nm)
LLA_8EO_{17}	S	3.1	5.4[e]	S	5.56 ± 0.01	4.6[e]
$LLA_{16}EO_5$	unstable/FB	na	na	unstable	na	na
$LLA_{16}EO_{11}$	FB/V	3.1	5.6[f]	V	156 ± 1	c.a. 5.9[f,h]
$LLA_{16}EO_{17}$	C	3.6	6.3[g]	C	na	6.6[g]
$LLA_{16}EO_{48}$	S	5.6	9.1[e]	S	10.08 ± 0.02	9.1[e,h] (4.5[h,i])

[a]Cross-sectional radius of the LLA core obtained by SCF. [b]Total hydrodynamic cross-sectional radius from SCF. [c]Hydrodynamic radius, measured by MA-DLS. [d]Cross-sectional radius, measured by SAXS. [e]Value refers to the radius of spherical micelle. [f]Value refers to the bilayers thickness. [g]Value refers to the cylindrical micelle cross sectional radius. [h]Average from three different concentrations. [i]Sphere core radius determined by SAXS.

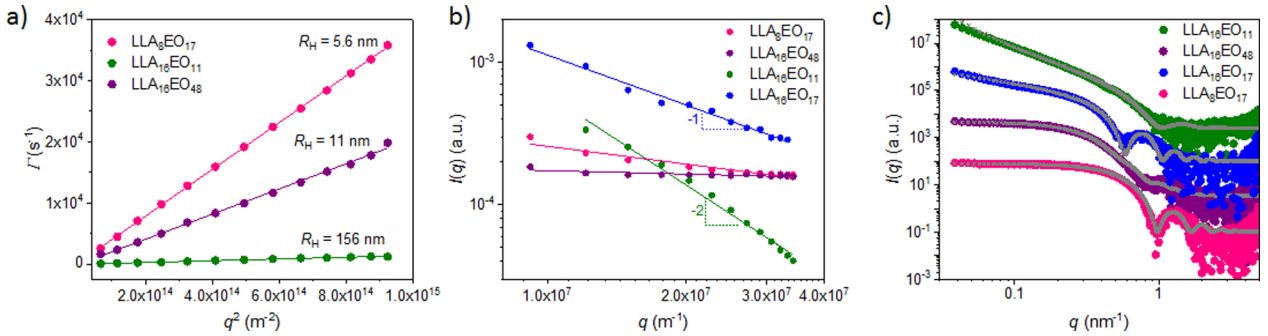

Figure 3. Scattering results of the self-assembled BCO library: (a) Γ vs q plot to determine the R_H of the spherical particles; (b) Scattering intensity I vs q to predict the shape of the self-assembled structures; (c) SAXS scattering profiles and corresponding fits. SAXS data is shifted vertically for clarity.

values, typical ethylene oxide scattering peaks are present, indicative for crystallization of the EO_{48} chain.[26,27] They overlay with the distinct peaks for the crystallization of the lactic acid block.

Subsequently, the self-assembly of these BCOs was studied in aqueous media. Here, the prediction of the thermodynamically most stable morphology and size by numerical SCF[20] lattice theory helped significantly in guiding the sample preparation (see SI for a detailed discussion).[13,29,30] SCF theory predicts the assembly of $LLA_{16}EO_n$ into spherical micelles for $y \geq 30$, cylindrical micelles are the most stable for $14 \leq y < 30$, and vesicular or bilayered structures are formed by copolymers with $y < 14$ (Figure 1c and Table 2). While micelles require a fast solvent switch, structures such as vesicles are formed upon slow switching of the solvent. The most reproducible sample preparation for micellar structures (LLA_8EO_{17}, $LLA_{16}EO_{48}$) was a quick injection of a THF stock solution into vortexing water. Only the injection into the vortex enabled a fast enough solvent switch to prevent the formation of other kinetically trapped states. Vesicular structures were formed upon dropwise addition of water to a THF stock solution using a syringe pump at 0.05 mL/min. Faster addition led to inhomogeneous samples. Other factors that influence the intermixing, such as reactor shape and stirring speed, did not show an effect. Cylindrical structures were prepared by dropwise addition of water to a THF stock solution while sonicating this mixture or with a syringe pump at 0.05 mL/min. It is important to note that the outcome of the sample preparation was sensitive to the aging and crystallinity of the bulk BCOs. All history of crystallinity had to be erased by rigorous dissolution prior to making samples in water. Only then it was possible to arrive at a reproducible sample preparation procedure (see SI for a detailed discussion).

Multiangle laser light scattering experiments were performed to measure the characteristic sizes and to obtain an indication of the morphology of the self-assembled structures. Interestingly, the hydrodynamic radius size (R_H) of the formed particles varies greatly (Figure 3a). $LLA_{16}EO_{11}$ yields the largest structures by far: R_H = 156 nm ($LLA_{16}EO_{11}$). The other BCOs are smaller: R_H = 11 nm ($LLA_{16}EO_{48}$) and R_H = 5.6 nm (LLA_8EO_{17}). A log−log representation of the complementary static light scattering data (Figure 3b) reveals distinct powerlaw scaling exponents m with $I \propto q^{-m}$ for LLA_8EO_{17} and $LLA_{16}EO_{48}$ ($m \sim 0$), $LLA_{16}EO_{11}$ ($m \sim 2$), and $LLA_{16}EO_{17}$ ($m \sim 1$), which are indicative for small (spherical), vesicular (lamellar), and cylindrical morphologies, respectively.[31]

The wider q-range accessible in small-angle X-ray scattering (SAXS) experiments allows to evaluate the structure of the assembled particles in greater detail (Figure 3c). The simplest possible form factor models were applied to accurately describe the data with the least possible fitting parameters (see SI). As expected, the SAXS profiles of LLA_8EO_{17} and $LLA_{16}EO_{48}$ were well captured by a homogeneous sphere and core−shell sphere form factor, respectively. The values obtained experimentally after the self-assembly in water correspond well to the simulated SCF results (R_{SCF} = 5.4 and 9.1 nm for LLA_8EO_{17} and $LLA_{16}EO_{48}$, respectively.) This indicates that the structures detected seem to be equilibrium micelles. Likewise, we find excellent agreement between the cross-sectional radii determined by SAXS and SCF ($R_{cs,SAXS}$ = 6.6 nm vs $R_{cs,SCF}$ = 6.3 nm) for the cylindrical $LLA_{16}EO_{17}$ micelles. Their length is beyond the resolution limit of the light and X-ray scattering experiments. A composite model comprising two form factors for a flat lamellar structure with a bilayer thickness of 5.9 nm

DOI: 10.1021/acsmacrolett.9b00814
ACS Macro Lett. 2020, 9, 38−42

(R_{SCF} = 5.6 nm) and spheres with dimensions >100 nm describes well the $LLA_{16}EO_{11}$ SAXS data in both the high and the low q-regimes. Without the spherical contribution, the model significantly deviated from the data in the low-q regime. This suggests that the bilayers predicted by SCF are present as spherical, vesicular architectures (rather than, e.g., flat or curved lamellae) in water. To corroborate the formation of closed spherical bilayers (vesicles), the particles formed by $LLA_{16}EO_{11}$ were visualized with total internal reflection fluorescence (TIRF) microscopy after addition of Nile Red (Figure S13). Nile Red is poorly soluble in water and tends to accumulate into hydrophobic domains where it becomes highly fluorescent.[32] Spherical particles, which do not interact with each other, were observed.

It is important to note that, although the SCF predictions do not take the possibility of crystallization in the LLA block into account, the predicted morphologies of our BCOs correspond well with to those experimentally observed (Table 2). To assess if the lactic acid part crystallizes in the core of the formed morphologies, $LLA_{16}EO_{11}$ was assembled at a high concentration to probe the presence of LLA crystallinity in the bilayer with micro-DSC.[33] In case of lamellar morphologies, crystallization has been shown to concur with phase segregation, resulting in long-range order and stable morphologies in bulk.[17] The solution was heated from 5 to 70 °C at a rate of 0.5 K min^{-1}. A sharp melting transition (T_m = 46 °C) was present in the heating run (Figure S13). Upon cooling, the sample partially precipitated, leading to a broad crystallization transition at around 32 °C. The melting temperature corresponds well with the melting in bulk (T_m = 50 °C) and with a melting in solution for a similar ABA system (T_m = 43 °C),[21] indicating that this transition is indeed due to LLA_{16} crystallization. For the other morphologies, it was not possible to reach the high concentrations required for micro-DSC experiments. As a result, it remains unclear if LLA crystallization also plays a role in the formation of spherical and cylindrical morphologies.

In summary, we have investigated the self-assembly in water of a series of discrete BCOs. SCF predictions guided the sample preparation procedures. The nature and sizes of the formed morphologies were in excellent agreement with the theoretically predicted ones. MicroDSC showed the presence of crystallized LLA in the bilayer of $LLA_{16}EO_{11}$. Despite this crystallinity, there was no mismatch between predicted and observed bilayer thickness. In this case, phase separation driven by the hydrophobic LLA block coincides with crystallization, resulting in stable morphologies.

Recent reports[18,19] on the dramatic impact of dispersity on the properties of low MW BCO self-assemblies, combined with lack in clarity on the consequences of crystallinity on the formation of spherical and cylindrical micelles, raises interest in studying both the effect of dispersity and crystallinity in the formation of nanostructures based on low MW BCOs in the future. This is the topic of our ongoing investigations.

■ ASSOCIATED CONTENT

Supporting Information

The Supporting Information is available free of charge at https://pubs.acs.org/doi/10.1021/acsmacrolett.9b00814.

Experimental procedures, synthesis and characterization data for all compounds, optimization of sample preparation, stability studies, and details about SCF computation and SAXS fitting (PDF)

■ AUTHOR INFORMATION

Corresponding Authors

*E-mail: k.milroy@gmx.net.
*E-mail: a.palmans@tue.nl.
*E-mail: e.w.meijer@tue.nl.

ORCID

Alessandro Ianiro: 0000-0003-4709-4350
Jose Rodrigo Magana: 0000-0001-8637-1467
Remco Tuinier: 0000-0002-4096-7107
Ilja K. Voets: 0000-0003-3543-4821
Anja R. A. Palmans: 0000-0002-7201-1548
E. W. Meijer: 0000-0003-4126-7492

Author Contributions

All authors have given approval to the final version of the manuscript.

Notes

The authors declare no competing financial interest.

■ ACKNOWLEDGMENTS

The authors acknowledge financial support from the Dutch Ministry of Education, Culture and Science (Gravity Program 024.001.035). This research received funding from The Netherlands Organization for Scientific Research (NWO) in the framework of the Programmatic Technology Area of the Fund New Chemical Innovations (TA 713.015.205). We are grateful to the BM29 beamline at the European Synchrotron Radiation Facilities (Grenoble, France) for access to the synchrotron facilities and Martha Brennich for help with acquiring SAXS data. We gratefully thank G. M. ter Huurne for his help of acquiring the SAXS data at the BM29 in Grenoble.

■ REFERENCES

(1) Tritschler, U.; Pearce, S.; Gwyther, J.; Whittell, G. R.; Manners, I. 50th Anniversary Perspective: Functional Nanoparticles from the Solution Self-Assembly of Block Copolymers. *Macromolecules* **2017**, *50*, 3439−3463.

(2) Schacher, F. H.; Rupar, P. A.; Manners, I. Functional Block Copolymers: Nanostructured Materials with Emerging Applications. *Angew. Chem., Int. Ed.* **2012**, *51*, 7898−7921.

(3) Elsabahy, M.; Heo, G. S.; Lim, S.-M.; Sun, G.; Wooley, K. L. Polymeric Nanostructures for Imaging and Therapy. *Chem. Rev.* **2015**, *115*, 10967−11011.

(4) Hamley, I. W. Nanotechnology with Soft Materials. *Angew. Chem., Int. Ed.* **2003**, *42*, 1692−1712.

(5) Blanazs, A.; Armes, S. P.; Ryan, A. J. Self-Assembled Block Copolymer Aggregates: From Micelles to Vesicles and Their Biological Applications. *Macromol. Rapid Commun.* **2009**, *30*, 267−277.

(6) Mai, Y.; Eisenberg, A. Self-Assembly of Block Copolymers. *Chem. Soc. Rev.* **2012**, *41*, 5969−5985.

(7) Zhulina, E. B.; Borisov, O. V. Theory of Block Polymer Micelles: Recent Advances and Current Challenges. *Macromolecules* **2012**, *45*, 4429−4440.

(8) Gröschel, A. H.; Schacher, F. H.; Schmalz, H.; Borisov, O. V.; Zhulina, E. B.; Walther, A.; Müller, A. H. E. Precise Hierarchical Self-Assembly of Multicompartment Micelles. *Nat. Commun.* **2012**, *3*, 710.

(9) Kempe, K.; Wylie, R. A.; Dimitriou, M. D.; Tran, H.; Hoogenboom, R.; Schubert, U. S.; Hawker, C. J.; Campos, L. M.; Connal, L. A. Preparation of Non-Spherical Particles from Amphiphilic Block Copolymers. *J. Polym. Sci., Part A: Polym. Chem.* **2016**, *54*, 750−757.

DOI: 10.1021/acsmacrolett.9b00814
ACS Macro Lett. 2020, 9, 38−42

(10) Leroux, J.-C. Editorial: Drug Delivery: Too Much Complexity, Not Enough Reproducibility? *Angew. Chem., Int. Ed.* **2017**, *56*, 15170−15171.
(11) Wauters, A. C.; Pijpers, I. A. B.; Mason, A. F.; Williams, D. S.; Tel, J.; Abdelmohsen, L. K. E. A.; van Hest, J. C. M. Development of Morphologically Discrete PEG−PDLLA Nanotubes for Precision Nanomedicine. *Biomacromolecules* **2019**, *20*, 177−183.
(12) Duan, X.; Li, Y. Physicochemical Characteristics of Nanoparticles Affect Circulation, Biodistribution, Cellular Internalization, and Trafficking. *Small* **2013**, *9*, 1521−1532.
(13) Ianiro, A.; Patterson, J.; García, Á. G.; van Rijt, M. M. J.; Hendrix, M. M. R. M.; Sommerdijk, N. A. J. M.; Voets, I. K.; Esteves, A. C. C.; Tuinier, R. A Roadmap for Poly(Ethylene Oxide)-Block-Poly-ε-Caprolactone Self-Assembly in Water: Prediction, Synthesis, and Characterization. *J. Polym. Sci., Part B: Polym. Phys.* **2018**, *56*, 330−339.
(14) van Genabeek, B.; de Waal, B. F. M.; Gosens, M. M. J.; Pitet, L. M.; Palmans, A. R. A.; Meijer, E. W. Synthesis and Self-Assembly of Discrete Dimethylsiloxane−Lactic Acid Diblock Co-Oligomers: The Dononacontamer and Its Shorter Homologues. *J. Am. Chem. Soc.* **2016**, *138*, 4210−4218.
(15) Oschmann, B.; Lawrence, J.; Schulze, M. W.; Ren, J. M.; Anastasaki, A.; Luo, Y.; Nothling, M. D.; Pester, C. W.; Delaney, K. T.; Connal, L. A.; McGrath, A. J.; Clark, P. G.; Bates, C. M.; Hawker, C. J. Effects of Tailored Dispersity on the Self-Assembly of Dimethylsiloxane−Methyl Methacrylate Block Co-Oligomers. *ACS Macro Lett.* **2017**, *6*, 668−673.
(16) van Genabeek, B.; de Waal, B. F. M.; Ligt, B.; Palmans, A. R. A.; Meijer, E. W. Dispersity under Scrutiny: Phase Behavior Differences between Disperse and Discrete Low Molecular Weight Block Co-Oligomers. *ACS Macro Lett.* **2017**, *6*, 674−678.
(17) van Genabeek, B.; Lamers, B. A. G.; de Waal, B. F. M.; van Son, M. H. C.; Palmans, A. R. A.; Meijer, E. W. Amplifying (Im)Perfection: The Impact of Crystallinity in Discrete and Disperse Block Co-Oligomers. *J. Am. Chem. Soc.* **2017**, *139*, 14869−14872.
(18) Sun, J.; Teran, A. A.; Liao, X.; Balsara, N. P.; Zuckermann, R. N. Crystallization in sequence-defined peptoid diblock copolymers induced by microphase separation. *J. Am. Chem. Soc.* **2014**, *136*, 2070−2077.
(19) Sun, J.; Teran, A. A.; Liao, X.; Balsara, N. P.; Zuckermann, R. N. Nanoscale phase separation in sequence-defined peptoid diblock copolymers. *J. Am. Chem. Soc.* **2013**, *135*, 14119−14124.
(20) Gangloff, N.; Höferth, M.; Stepanenko, V.; Sochor, B.; Schummer, B.; Nickel, J.; Walles, H.; Hanke, R.; Würthner, F.; Zuckermann, R. N.; Luxenhofer, R. Linking Two Worlds in Polymer Chemistry: The Influence of Block Uniformity and Dispersity in Amphiphilic Block Copolypeptoids on Their Self-Assembly. *Biopolymers* **2019**, *110*, e23259.
(21) Das, A.; Petkau-Milroy, K.; Klerks, G.; van Genabeek, B.; Lafleur, R. P. M.; Palmans, A. R. A.; Meijer, E. W. Consequences of Dispersity on the Self-Assembly of ABA-Type Amphiphilic Block Co-Oligomers. *ACS Macro Lett.* **2018**, *7*, 546−550.
(22) Fleer, G. J.; Cohen Stuart, M. A.; Scheutjens, J. M. H. M.; Cosgrove, T.; Vincent, B. *Polymers at Interfaces*; Springer: Netherlands, 1993.
(23) Takizawa, K.; Nulwala, H.; Hu, J.; Yoshinaga, K.; Hawker, C. J. Molecularly Defined (L)-Lactic Acid Oligomers and Polymers: Synthesis and Characterization. *J. Polym. Sci., Part A: Polym. Chem.* **2008**, *46*, 5977−5990.
(24) van Nostrum, C. F.; Veldhuis, T. F. J.; Bos, G. W.; Hennink, W. E. Hydrolytic Degradation of Oligo(Lactic Acid): A Kinetic and Mechanistic Study. *Polymer* **2004**, *45*, 6779−6787.
(25) Tam, Y. T.; Gao, J.; Kwon, G. S. Oligo(Lactic Acid)n-Paclitaxel Prodrugs for Poly(Ethylene Glycol)-Block-Poly(Lactic Acid) Micelles: Loading, Release, and Backbiting Conversion for Anticancer Activity. *J. Am. Chem. Soc.* **2016**, *138*, 8674−8677.
(26) Takahashi, Y.; Tadokoro, H. Structural Studies of Polyethers, (−(CH2)m−O−)n. X. Crystal Structure of Poly(Ethylene Oxide). *Macromolecules* **1973**, *6*, 672−675.
(27) Kripotou, S.; Psylla, C.; Kyriakos, K.; Raftopoulos, K. N.; Zhao, J.; Zhang, G.; Pispas, S.; Papadakis, C. M.; Kyritsis, A. Structure and Crystallization Behavior of Poly(Ethylene Oxide) (PEO) Chains in Core-Shell Brush Copolymers with Poly(Propylene Oxide)-Block-Poly(Ethylene Oxide) Side Chains. *Macromolecules* **2016**, *49*, 5963−5977.
(28) Tsuji, H. Poly(Lactide) Stereocomplexes: Formation, Structure, Properties, Degradation, and Applications. *Macromol. Biosci.* **2005**, *5*, 569−597.
(29) Hurter, P. N.; Scheutjens, J. M. H. M.; Hatton, T. A. Molecular Modeling of Micelle Formation and Solubilization in Block Copolymer Micelles. 1. A Self-Consistent Mean-Field Lattice Theory. *Macromolecules* **1993**, *26*, 5592−5601.
(30) Lebouille, J. G. J. L.; Tuinier, R.; Vleugels, L. F. W.; Cohen Stuart, M. A.; Leermakers, F. A. M. Self-Consistent Field Predictions for Quenched Spherical Biocompatible Triblock Copolymer Micelles. *Soft Matter* **2013**, *9*, 7515−7525.
(31) Hammouda, B. A new Guinier−Porod model. *J. Appl. Crystallogr.* **2010**, *43*, 716−719.
(32) Dutta, A. K.; Kamada, K.; Ohta, K. Spectroscopic Studies of Nile Red in Organic Solvents and Polymers. *J. Photochem. Photobiol., A* **1996**, *93*, 57−64.
(33) Zinn, T.; Willner, L.; Lund, R. Nanoscopic Confinement through Self-Assembly: Crystallization within Micellar Cores Exhibits Simple Gibbs-Thomson Behavior. *Phys. Rev. Lett.* **2014**, *113*, 238305.

DOI: 10.1021/acsmacrolett.9b00814
ACS Macro Lett. 2020, 9, 38−42